

Strangeness, charm, and bottom production from dense parton matter in high energy nuclear collisions

K. Geiger

School of Physics and Astronomy, University of Minnesota, Minneapolis, Minnesota 55455

(Received 8 April 1993; revised manuscript received 6 July 1993)

The production properties of strange, charm, and bottom quarks in ultrarelativistic $A + A$ collisions at heavy ion colliders are investigated for systems from $p + p$ to Au+Au in the energy range $\sqrt{s}/A = 200\text{--}6300$ GeV, using the parton cascade model. Within this kinetic space-time description of the parton dynamics, based on the current understanding of semihard and hard QCD interactions, it is found that a substantial enhancement of s , c , and b production can be expected in AA collisions *with* plasma formation of the deconfined parton matter relative to the case of a purely hadronic scenario *without* plasma formation. Because of the large number of initially produced energetic gluons the main contribution comes from decays of virtually excited gluons and gluon fusion. The associated resonance production of ϕ , J/ψ , and Υ is estimated and it is shown that the resulting abundances of these vector mesons can be used as a sensitive thermometer of the hot and dense QCD matter formed in the central region during the very early stage of the collisions. Therefore the future heavy ion collider experiments would have an attractive opportunity to probe the evolution of partons through preequilibrium toward plasma formation by measuring the multiplicities and momentum spectra of heavy mesons.

PACS number(s): 25.75.+r, 12.38.Bx, 12.38.Mh, 24.85.+p

I. INTRODUCTION

The expected formation of hot and ultradense matter in the central region of high energy heavy ion collisions at the planned BNL Relativistic Heavy Ion Collider (RHIC) and the CERN Large Hadron Collider (LHC) offers the opportunity to study QCD in a large volume at high energy densities. The search for experimental evidence for the predicted QCD phase transition to a locally deconfined quark-gluon plasma (QGP) [1–3] during the very early stage of the reactions requires to extract unambiguous characteristic signals [4–6] that survive the complex evolution through the later stages of the collision. In this context the microscopic dynamics of partons in these nuclear collisions during the first few fm has recently attracted growing interest. A number of investigations [7–11] addressing the mechanisms that precede the formation of a thermalized QGP have led to considerable progress in understanding the very early stage of the reactions. It was realized that the *preequilibrium* phase, from the moment of nuclear contact to the establishment of a locally thermalized plasma of partons, may significantly influence the yield of some typical QGP signatures, such as dileptons, direct photons, and hadrons containing strange, charm, or bottom quarks. The kinetics of interacting quarks and gluons during this early stage of nuclear collisions and the space-time evolution of the parton distributions has been studied in detail in Refs. [10,11] within the *parton cascade model* [12,13]. This approach is a perturbative QCD-based kinetic description of the partons' phase-space evolution in real time. It allows to evolve the initial partons in the colliding nuclei smoothly from their first hard scatterings through the preequilibrium stage into a fully thermalized

plasma by “solving” an appropriate relativistic transport equation with Monte Carlo methods. Based on these investigations, and on other analyses [8,9,14,15], the current understanding of the partons' evolution in high energy nuclear collisions during the first few fm after the nuclear contact at τ_c may be summarized in four stages [2,9] (here $\tau_c < 0$, with $|\tau_c| \simeq 0.5\text{--}1$ fm, is defined such that $\tau = 0$ is the moment of maximum nuclear overlap [10]).

(i) $\tau_c \leq \tau \lesssim 0.2$ fm: The vehement materialization of initial virtual partons plus associated gluon emission produces most of the entropy and results in a large number of “few GeV” excitations, which are mostly gluons.

(ii) $0 \lesssim \tau \lesssim 0.3$ fm: Both the gluons and quarks rapidly reach a local kinetic equilibrium in the central collision region with approximately isotropic momentum distributions in the local rest frame of the matter.

(iii) $0.3 \lesssim \tau \lesssim 2$ fm: The gluons approach complete equilibration—the saturation of the phase-space density toward its chemical equilibrium value. The phase-space population of quarks evolves significantly slower, mostly by gluon induced processes, and yields at most 1/2 to 2/3 of the quarks' chemical equilibrium densities.

(iv) $\tau \gtrsim 2$ fm: The gluon-dominated plasma expands and cools without further significant change of its chemical composition.

Thus, the early evolution of these nuclear collisions is governed by the dominant role of gluons, due to their large interaction probability and the large gluonic component in the initial nuclear wave functions. This leads to a “hot glue scenario” [7], in which the large number of initially produced energetic partons create a high temperature, high density plasma of predominantly hot gluons and a considerably smaller number of quarks. Figure 1

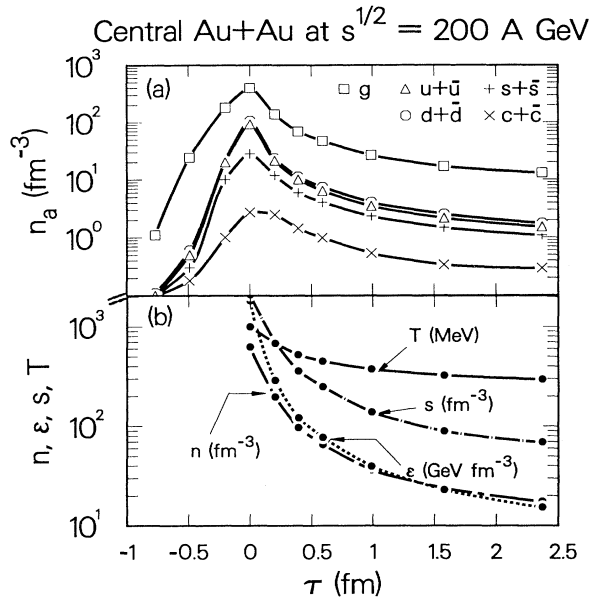


FIG. 1. Characteristic space-time evolution of the parton system in Au+Au collisions at $\sqrt{s} = 200$ A GeV as a function of proper time τ in the central region with space-time rapidity $|\eta| \leq 1$ and transverse radius $|r_{\perp}| \leq 5$ fm: (a) Development of the local number densities of gluons, n_g and of quarks plus antiquarks $n_q + n_{\bar{q}}$. Only the valence quarks and those partons that have interacted at least once or have been created in pair production processes are taken into account, since these contribute to the entropy production; (b) time evolution of *total* parton density n , energy density ϵ , entropy density s and of the associated temperature $T = \frac{4}{3}(\epsilon/s)$ in the central region.

shows, as an exemplary illustration of the partons' space-time evolution, the development of the gluon and quark number densities in the central collision region of zero impact Au+Au reactions at RHIC energy, as well as the total number, energy, and entropy densities and the associated temperature of the system [11]. Such extreme conditions are expected to significantly influence QGP signals and should modify the observable consequences for the production of particles at early times. In this context, the production of dileptons and of direct photons from the preequilibrium stage recently have been investigated [16,17], with the common general conclusion that the particle yield from the early stage is significant.

The aim of the present paper is to extract and analyze, within the kinetic approach of the parton cascade model, the properties of heavy quark production (strange, charm, as well as bottom quarks and antiquarks) in ultrarelativistic nuclear collisions. Particular emphasis lies on heavy ion collisions at RHIC and LHC energies, for which I estimate the resulting production rates of ϕ , J/ψ , ψ' , and Υ mesons as characteristic QGP signatures.

Investigations of the properties of strangeness and charm production in high energy heavy ion reactions led to expectations of potentially observable enhanced strange hadron production [18,19] and J/ψ suppression

[20,21], respectively. The enhanced abundance of strange particles is expected to be a good indicator for the establishment of a thermalized QGP, because for plasma temperatures $T \gg m_s$ ($m_s \simeq 150$ MeV) there should be no significant difference between u , d , and s quark production. The idea of a suppression of $c\bar{c}$ mesons J/ψ , ψ' , on the other hand, is based on the notion that $c\bar{c}$ pairs are produced mainly via primary hard collisions of energetic gluons during the preequilibrium stage up to shortly after the plasma formation (before the initial temperature of the plasma drops below the production threshold), and the J/ψ , ψ' mesons formed from these pairs may subsequently experience deconfinement when traversing the region of the plasma. Additional charm production in the plasma at later times would not occur due to the large charm quark mass ($m_c \simeq 1.3\text{--}1.5$ GeV) and the rapidly dropping temperature. Similar arguments hold for even heavier particles, such as the $b\bar{b}$ meson Υ . However there are other estimates [22,23] that predict, instead of a suppression, rather an enhancement of J/ψ production in the plasma, because of the possibility of having several charmed quarks produced independently in close proximity of phase space.

The issue of charm production from partons in heavy ion collisions as a QGP signal has recently been addressed in Refs. [7,8,24]. In particular the thermal versus purely hadronic production was studied in detail by Shor [24]. In this investigation the procedure was, to (i) calculate the direct $c\bar{c}$ production via gluon fusion or $q\bar{q}$ annihilation in pp collisions and extrapolating to AA collisions, (ii) to estimate the thermal rate by *assuming* QGP formation, and, (iii) to compare the two yields to obtain information about the characteristics of a thermalized QGP relative to a scenario without plasma formation. However, in such an analysis there are at least two major uncertainties involved. First, the thermal production depends sensitively on the choice of the formation time and the initial temperature of the plasma. Second, although quark production is well understood in hadron-hadron collisions within perturbative QCD, the increasing (with beam energy \sqrt{s} and mass number A) importance for the reaction dynamics of nuclear and dense medium effects are very likely to alter the simple extrapolation of the resulting particle yields from pp to AA with a typical scaling behavior $\propto A^{1-1}$, independent of \sqrt{s} [25]. Generally one might expect from collective effects a multiplicity dependence that scales $\propto A^k \alpha_P(s)$, with $k=1$ (2) for pA (AA) and $2/3 \leq \alpha_P \leq 4/3$, depending on the particle species P as well as on s [26].

Furthermore, a common approximation when estimating heavy quark production and resulting hadron yields in nuclear collisions is the restriction to *flavor creation* processes and the neglect of *flavor excitation* processes by which initial virtual quarks are scattered out of the initial sea quark distribution of the colliding nuclei to become "real" excitations. The yield of such s , c , and b quarks depends on the initial strangeness, charm, and bottom content in the nuclear structure functions. Since these components increase with beam energy, and since the cross sections for the flavor excitation processes are comparably large [27], this additional source is essential

to include in the consideration.

With the parton cascade model [12,13] it is possible to resolve these shortcomings and to systematically investigate the beam energy and mass dependence of heavy quark production, extract formation times, and associated initial plasma temperatures, as well as to separate the individual processes that contribute. In this paper I report on calculations within this model of strangeness, charm, and bottom production in central AA collisions from $A=1-197$ in the energy range between RHIC and LHC ($\sqrt{s}/A = 200-6300$ GeV). For the case of heavy ion reactions, two different scenarios are compared. The first scenario considers Au+Au collisions *with* plasma formation by realistic simulation including nuclear and dense medium effects [13,28], such as nuclear shadowing [29], enhanced multiple minijet production [30,31], parton cascading with rescattering, emission and absorption [10], and the Landau-Pomeranchuk-Migdal effect [32]. The second scenario mimics Au+Au collisions *without* plasma formation, on the basis of purely hadronic interactions, by simulating pp collisions and multiplying with the expected average number of nucleon-nucleon scatterings in these reactions. The results imply a substantial enhancement of strange, charm, as well as bottom particle yields in AA reactions relative to pp collisions and are consistent with the formation of a high temperature gluon-dominated plasma in the central region within already $\simeq 0.2-0.3$ fm after the moment of maximum nuclear overlap found in earlier investigations [9–11]. Especially the intense production of charm and the associated abundance of D and J/ψ mesons (in contrast with J/ψ suppression) should provide an observable signal in the invariant mass spectrum of lepton pairs resulting from the decays of these mesons. It will be shown that this can serve as a sensitive thermometer of the initial temperature of the parton matter upon the time of plasma formation. At LHC energies even the bottom mesons B and Υ are produced copiously enough to be measurable with sufficiently good statistics.

I would like to stress beforehand that the calculations and results presented in this paper must be viewed as an optimistic upper limit of the possible flavor yield that is subject to considerable uncertainties (as will be discussed in Sec. III G). It is entirely possible that once more experimental and theoretical information is available regarding the heavy flavor sea excitation and glue decay production at RHIC and LHC energies, these mechanisms which are found theoretically to be clearly dominating, may lose in importance. Although I intend to stimulate consideration of experiments on, e.g., D meson detection as a signature for copious charm production, I emphasize that the theoretical predictions of this work should not lead to premature conclusions for the experimentally observable yield.

The remainder of the paper is structured as follows. In Sec. II the statistical framework for the space-time description of the parton kinetics is briefly reviewed and the method of calculating the quark production rates from the evolution of parton cascades is introduced. Section III is devoted to a detailed presentation of results from simulations of AA collisions in the energy range

$\sqrt{s}/A = 200-6300$ GeV. The different production mechanisms for strange, charm, and bottom quarks, the resulting multiplicities as well as momentum spectra are discussed, and corresponding initial plasma temperatures are inferred. Furthermore the A dependence of the quark yields is investigated in terms of a power-law scaling behavior. Finally the resonance production rates for the vector mesons ϕ , J/ψ , ψ' , and Υ are extracted from the coalescence probabilities of quarks and antiquarks with the required flavors. The observable consequences for the resonance production at the RHIC and LHC heavy ion experiments are elucidated by estimating the count rates of muon pairs produced by the decays of these mesons. Section IV is reserved for a summary and some concluding remarks.

II. QUARK FLAVOR PRODUCTION FROM CASCADING PARTONS

A detailed description of the parton cascade model can be found in Refs. [12,13]. In this model, ultrarelativistic nuclear collisions are described as the time evolution of the partons' phase-space distributions. The space-time development is formulated within renormalization-group-improved QCD perturbation theory, embedded in the framework of relativistic transport theory. The dynamics of the dissipative processes during the early stage of a nuclear reaction is simulated as the evolution of multiple interrelated parton cascades associated with quark and gluon interactions. At the end of the perturbative QCD phase, hadronization is modeled as a recombination of the final state partons to form color singlet clusters, followed by the fragmentation of these clusters into observable hadronic states.

In extracting the space-time history of the production of heavy quarks (antiquarks) Q (\bar{Q}) from the partons' evolution, each parton cascade is decomposed in a number of elementary processes that determine the net yield of Q or \bar{Q} through their detailed balance.

(i) The *flavor creation (annihilation)* processes by which a $Q\bar{Q}$ pair is newly created (annihilated) through quark-antiquark annihilation, gluon fusion, or virtual gluon decay:

$$q + \bar{q} \leftrightarrow Q + \bar{Q}, \quad (1)$$

$$g + g \leftrightarrow Q + \bar{Q}, \quad (2)$$

$$g^* \leftrightarrow Q + \bar{Q}, \quad (3)$$

where $q = u, d, s, c, b$ and $Q = s, c$ or b .

(ii) The *flavor excitation* processes in which a Q or a \bar{Q} is knocked out of the sea of one of the incoming nuclei by a collision with a q , \bar{q} , or g :

$$q(\bar{q}) + Q(\bar{Q}) \rightarrow q(\bar{q}) + Q(\bar{Q}), \quad (4)$$

$$g + Q(\bar{Q}) \rightarrow g + Q(\bar{Q}). \quad (5)$$

It is important to realize that the subset of processes (1)–(5) is much more general than it seems at first sight. In the parton cascade model the complicated space-

time structure of multiple parton interactions is pictured as many interrelated cascades composed of elementary $2 \rightarrow 2$ collisions, $2 \rightarrow 1$ fusion processes, and $1 \rightarrow 2$ branchings, plus higher order virtual and real corrections [13]. The decomposition into the elementary processes (1)–(5) is simply a convenient accounting prescription for the different production mechanisms [17]. In fact, all kinds of higher order processes are taken into account. For example, the process $g + g \rightarrow Q + \bar{Q} + g + g$ is included in the form of two gluon annihilation into a $Q\bar{Q}$ pair, where the Q (\bar{Q}) emits two bremsstrahlung gluons, or both Q and \bar{Q} emit a single gluon. Similarly, processes with three or more partons in the initial state are also accounted for. For instance, the process $Q + g + g \rightarrow Q + g$ is decomposed into the absorption of the first gluon by the second and the subsequent collision of the quark Q with the excited gluon.

Within this framework the space-time history of Q (\bar{Q}) production via (1)–(5) in a nuclear collision is extracted from the time development of the phase-space distributions $F_a(p, r)$ for the partons of species $a = q_f, \bar{q}_f, g$ (f labeling the quark flavors), starting from their given initial form at time $t = t_0$ when the two nuclei begin to overlap. The time evolution is governed by the relativistic invariant transport equation [13] (natural units $\hbar = c = 1$ will be employed throughout)

$$p^\mu \partial_\mu F_a(p, r) = \sum_{\text{processes } k} I_a^{(k)}(p, r) \quad , \quad (6)$$

with a collision kernel $\sum I_a = \sum \{I_a^{\text{(gain)}} - I_a^{\text{(loss)}}\}$ on the right-hand side that balances the various processes

k by which a parton of type a with four-momentum $p \equiv p^\mu = (E, \mathbf{p})$ and space-time point $r \equiv r^\mu = (t, \mathbf{r})$ may be gained or lost in a phase-space volume $d^3p d^3r$ centered at \mathbf{p} and \mathbf{r} at time t . The collision kernel is a sum over Lorentz invariant collision integrals $I_a^{(k)}$ that involve the matrix elements for the different kind of interaction processes k in which at least one parton of type a is involved. The initial phase-space distribution of partons in the incoming nuclei at time $t = t_0$ (the moment of nuclear contact), $F_a(p, r)|_{t=t_0} \equiv F_a^{(0)}(p, r, Q_0^2)$, is constructed as a convolution of the scale (Q_0^2) dependent nuclear structure functions with a spatial distribution determined by the nucleons' elastic form factor. The effect of parton shadowing, evident in the observations of the European Muon Collaboration (EMC) [33] as a depletion of soft partons in a nucleus relative to a nucleon, is accounted for in a shadowing factor by employing the prescription described in Refs. [13,31].

From Eq. (6) one obtains the following rate equations (one for each parton species a) by integrating over \mathbf{p} :

$$\partial_\mu n_a^\mu(r) = R_a^{\text{gain}}(r) - R_a^{\text{loss}}(r) \equiv R_a(r) \quad , \quad (7)$$

where

$$n_a^\mu(r) = \gamma_a \int \frac{d^3p}{(2\pi)^3 E} p^\mu F_a(r, p) \quad (8)$$

are the local space-time-dependent parton currents. The factors γ_a are the products of spin and color degeneracies ($\gamma_g = 2 \times 8$ for gluons and $\gamma_q = \gamma_{\bar{q}} = 2 \times 3$ for quarks and antiquarks). The quantity

$$\begin{aligned} R_a(r) &= \sum_{\text{processes } k} \int \frac{d^3p}{(2\pi)^3 E} \left[I_a^{\text{gain}(k)}(r, p) - I_a^{\text{loss}(k)}(r, p) \right] \\ &= \sum_{\text{processes } k} \frac{1}{S_a} \int \prod_{i=1}^{n+m} \frac{d^3p_i}{(2\pi)^3 E_i} |\mathcal{M}_{\text{eff}}^{(k)}|^2 (2\pi)^4 \delta^4 \left(\sum_{i=1}^n p_i - \sum_{j=n+1}^{m+n} p_j \right) \prod_{i=1}^n F_i(r, p_i) \prod_{j=n+1}^{m+n} [1 + \theta_j F_j(r, p_j)] \end{aligned} \quad (9)$$

is the net gain rate for producing a parton a at $r = (t, \mathbf{r})$ through any of the considered processes k . The spin- and color-averaged effective matrix elements squared, $|\mathcal{M}_{\text{eff}}^{(k)}|^2$, take into account higher order QCD corrections to the first order Born terms [10,13], are weighted by distribution functions F_i for the particles coming in [$1 + \theta_j F_j$] for the particles going out of the vertex, where $\theta_j = -1$ for fermions and $\theta_j = +1$ for bosons. The statistical factor S_a is given by $S_a = \prod \nu_a^{\text{in}}! \nu_a^{\text{out}}!$ when there are ν_a^{in} (ν_a^{out}) identical particles of species a in the initial (final) state. The specific forms of the effective matrix elements squared $|\mathcal{M}_{\text{eff}}^{(k)}|^2$ were derived in Ref. [10] in terms of lowest order perturbative QCD interaction Born amplitudes which are squared and weighted with a form factor for each of the partons coming in and going out of the vertex. The form factors, which inclusively

sum up the higher order corrections associated with the leading logarithmic collinear and infrared singularities of QCD give the probability for additional gluon emission through QCD bremsstrahlung and are taken into account as radiative emissions of both spacelike and timelike partons [10,13]. The effective matrix elements are embedded in the collision term of the transport equation (6) and generate the space-time evolution of the partons' phase-space distributions $F_a(p, r)$ as a succession of multiple parton-parton collisions together with associated radiative emissions (branchings) and absorption (fusion) processes, once the incoming nuclear clouds begin to overlap. This concept and the Monte Carlo procedure for this simulation is described in detail in Ref. [13].

According to the outlined concept, I will be concerned in the following only with the subset of interaction pro-

cesses (1)–(5), in which an interaction of any kind of parton a results in the production or annihilation of a heavy quark $Q = s, c, b$ or antiquark \bar{Q} . Thus, the total net production rate for quarks Q (and similar for antiquarks \bar{Q}) is

$$R_Q(\tau) = \sum_{a,b} \left[R_{ab \rightarrow Q\bar{Q}} - R_{Q\bar{Q} \rightarrow ab} \right] + \left[R_{g \rightarrow Q\bar{Q}} - R_{Q\bar{Q} \rightarrow g} \right] + \sum_a R_{aQ^{(\text{prim})} \rightarrow aQ} \quad , \quad (10)$$

corresponding to the sum of net rates for the flavor creation processes (1)–(3) via $Q\bar{Q}$ production and the flavor excitation processes via scatterings of primary Q out of the coherence of the initial nuclear wave functions (indicated by the label “prim”). The rates $R_{i \rightarrow f}$ on the right-hand side are extracted from the parton cascade simulation, evaluated according to Eqs. (6)–(9), using the “massive” Q production amplitudes derived by Combridge [27] in the effective matrix elements \mathcal{M}_{eff} of Eq. (9). The matrix elements are calculated with the standard running QCD coupling strength $\alpha_s(k^2)$ at $k^2 = (p_Q + p_{\bar{Q}})^2 = \hat{s}$ for the processes $ab \leftrightarrow Q\bar{Q}$, at $k^2 = p_g^2$ for $g^* \leftrightarrow Q\bar{Q}$, and at $k^2 = 1/2(p_a + p_Q)^2 = \hat{s}/2$ for $aQ \rightarrow aQ$. The current quark masses are taken to be $m_u = 5.6$ MeV, $m_d = 9.9$ MeV, $m_s = 199$ MeV, $m_c = 1.35$ GeV, and $m_b = 5$ GeV. Furthermore a K factor ($K \simeq 2$) is included for primary parton collisions to account for next-to-leading order corrections to the parametrization of the initial nuclear structure functions by adopting the prescription of Ref. [34].

To make connection with experimental quantities, the total rest-frame rates $R_Q(\tau)$ and $R_{\bar{Q}}(\tau)$ must be convoluted over the space-time history of the parton system, since detectors record particle multiplicities only in a space-time-integrated way. Using $d^4r = \tau d\tau d\eta d^2r_\perp$, where τ is the proper time, η the space-time rapidity, and \mathbf{r}_\perp the transverse coordinate, the experimentally relevant, space-time integrated number distribution of produced Q and \bar{Q} with respect to their center-of-mass rapidity y is obtained by

$$\frac{dN_{Q+\bar{Q}}}{dy} = \int \tau d\tau d\eta d^2r_\perp \frac{d}{dy} \{ R_Q(\tau) + R_{\bar{Q}}(\tau) \} \quad (11)$$

Thus, the Q plus \bar{Q} yield from the various processes (1)–(5) is accumulated by summing over the complete space-time evolution of the parton system in phase space up to a certain time τ .

III. HEAVY QUARK PRODUCTION IN CENTRAL AA COLLISIONS BETWEEN RHIC AND LHC ENERGIES

The results presented and discussed in this section were obtained by following the parton cascade development of the nuclear collisions in full six-dimensional phase-space

and the proper time $\tau = \text{sgn}[t - t_0(s)] \sqrt{[t - t_0(s)]^2 - z^2}$, where t is the center-of-mass time and $t_0(s)$ is its value at the moment of maximum overlap of the colliding nuclei, ranging from $t_0 \simeq 0.9$ fm for $\sqrt{s} = 200$ A GeV to $t_0 \simeq 0.4$ fm for $\sqrt{s} = 6300$ A GeV [10,11]. Thus, in the center of mass, at $z = 0$, the initial nuclear contact occurs at $\tau = -t_0(s)$ and the maximum density is achieved at $\tau \simeq 0$. A series of simulations of AA collisions were performed, with $A = 1, 32, 56, 108, 197$ at various beam energies $\sqrt{s} = 200, 1000, 2000, 4000, 6300$ A GeV, except for pp collisions, for which $\sqrt{s} = 200, 540, 900, 1800, 6300$ GeV was chosen. All AA calculations were carried out with zero impact parameter, whereas for pp collisions it was averaged over impact parameters, because in nuclear collisions with $A > 1$, the nucleons have different impact parameters, even when the nuclei collide head on.

It has to be stressed at this point that the optimistic predictions on strange, charm, and bottom production presented below rely on the underlying assumption of the parton cascade model, that the nuclear dynamics during the first few fm can be essentially described on the basis of perturbative QCD, in terms of multiple binary parton-parton collisions and associated intertwined cascades (for a discussion of the limitations and open questions of the model, see Ref. [13]). The characteristics of the partons’ space-time evolution therefore depends on the chosen boundary between perturbative and non-perturbative regimes, which is set by two infrared cut-off parameters, one for the momentum transfer in parton collisions, $p_{\perp \text{cut}}$, and one for the timelike virtual mass of cascading partons produced in radiative emissions, μ_{cut} . Although these parameters have been adjusted [13,35] to reproduce a wide range of experimental data from high energy pp ($p\bar{p}$) collisions and e^+e^- annihilation, it remains to investigate in detail how these parameters are affected in heavy ion collisions by nuclear and dense medium effects. It is expected [2] that the color screening length and effective medium-induced masses of gluons and quarks should provide a natural regularization of the perturbative QCD divergences. Eventually these quantities will need to be calculated dynamically as a function of space-time. For now, in the calculations presented here, the infrared cutoffs have been taken to be the same for pp and AA collisions [13]. However, particularly for $c\bar{c}$ and $b\bar{b}$ production the values of the cutoff parameters $p_{\perp \text{cut}}$ and μ_{cut} are not very influential, since for these processes the interaction scale is set by the partons invariant mass ($\sqrt{\hat{s}}$ or M_{g^*}) which has to be larger than the threshold $2m_{c(b)}$, whereas the cutoffs are set at $p_{\perp \text{cut}}(s) = 1.6\text{--}4.0$ GeV ($\sqrt{s} = 200\text{--}6300$ A GeV) and $\mu_{\text{cut}} = 1$ GeV.

A. Multiplicities

Figure 2 shows the central rapidity density $dN_{Q+\bar{Q}}/dy|_{y=0}$ versus the normalized beam energy \sqrt{s}/A of produced strange, charm, and bottom quarks plus antiquarks ($Q = s, c, b$) in central Au+Au collisions *with* [Fig. 2 (a)] and *without* [Fig. 2 (b)] plasma formation. The data points are the results of the simulations at vari-

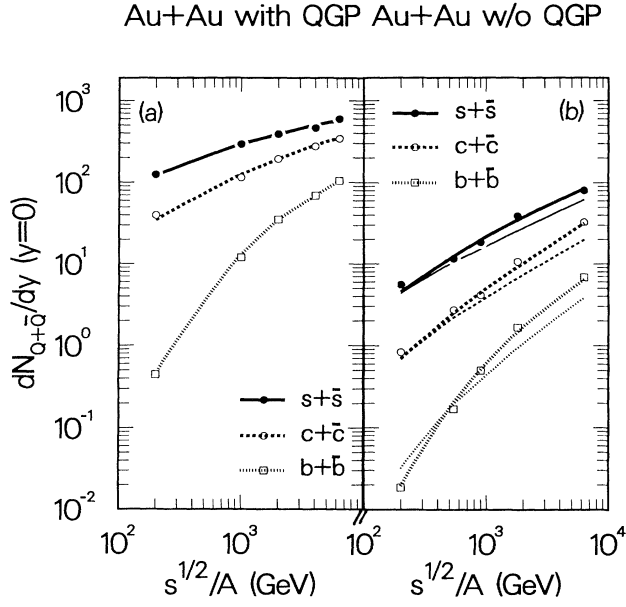


FIG. 2. Central rapidity density $dN_{Q+\bar{Q}}/dy|_{y=0}$ versus \sqrt{s}/A of produced strange, charm, and bottom quarks plus antiquarks ($Q = s, c, b$) in central Au+Au collisions: (a) *with* plasma formation, as obtained from the parton cascade simulations of Au+Au collisions on the basis of Eq. (11); (b) *without* plasma formation, as calculated from pp collisions and scaled to AA according to Eq. (13). The solid lines are the parton cascade results, and the thin lines are the corresponding simple parton model predictions, obtained by convoluting the proton structure functions with the quark production cross sections and taking into account only primary parton-parton collisions without subsequent cascading and gluon bremsstrahlung.

ous collider energies; the lines are interpolations to guide the eye.

In Fig. 2(a) the displayed energy dependence of $dN_{Q+\bar{Q}}/dy$ with plasma formation was obtained on the basis of Eq. (11). As has been found in Refs. [10,11], the parton system evolves rapidly through a preequilibrium stage toward a thermalized, gluon dominated plasma and establishes an approximate kinetic equilibrium in the central region already within $\tau \simeq 0.3$ fm after the moment of maximum nuclear overlap.

In Fig. 2(b) shows the purely hadronic production, *without* plasma formation, which was mimicked by simulating pp collisions, averaging over impact parameter, and, following Ref. [24], simply scaling the calculated multiplicities to Au+Au according to [36,38]

$$\frac{dN_{Q+\bar{Q}}^{AA}}{dy} = A^{\alpha+1/3} \frac{dN_{Q+\bar{Q}}^{pp}}{dy} \quad (12)$$

with $\alpha = 0.76$ [37].

As a consistency check, Fig. 2(b) also indicates the simple parton model result [24,27] (thin lines), evaluated for pp collisions and scaled to Au+Au, by convoluting the proton structure functions with the production cross

sections for the processes (1), (2), (3), and (5). This case corresponds to taking into account only primary parton-parton collisions without subsequent cascading and gluon bremsstrahlung. Evidently, in the case of hadronic production, the parton cascade result generally agrees with the simple parton model estimate, although a steadily growing deviation with \sqrt{s}/A from the parton model prediction is obvious. The stronger increase within the parton cascade model arises, because multiple parton scatterings and $Q\bar{Q}$ production by radiative gluons from parton cascades play an increasingly important role, even in hadron collisions.

Comparing the two scenarios with and without plasma formation, Figs. 2(a) and 2(b), respectively, one observes a substantial enhancement of more than one order of magnitude of the quark production for all three flavors s , c , and b . Note that this enhancement comes on top of a substantial depletion of partons in the central rapidity region due to nuclear shadowing of the initial gluon and quark distributions and due to the medium effects discussed in [13,28].

Figure 3 displays, in correspondence to Fig. 2(a), the individual contributions from the processes (1)–(5) to the central rapidity density of strange [Fig. 3(a)] and charm quarks plus antiquarks [Fig. 3(b)] as a function of \sqrt{s}/A . Most significant is the strongly increasing yield from the flavor creation processes involving gluons, $g^* \rightarrow Q\bar{Q}$, and $gg \rightarrow Q\bar{Q}$. In particular the $Q\bar{Q}$ production by hard bremsstrahlung gluons g^* is mainly responsible for the

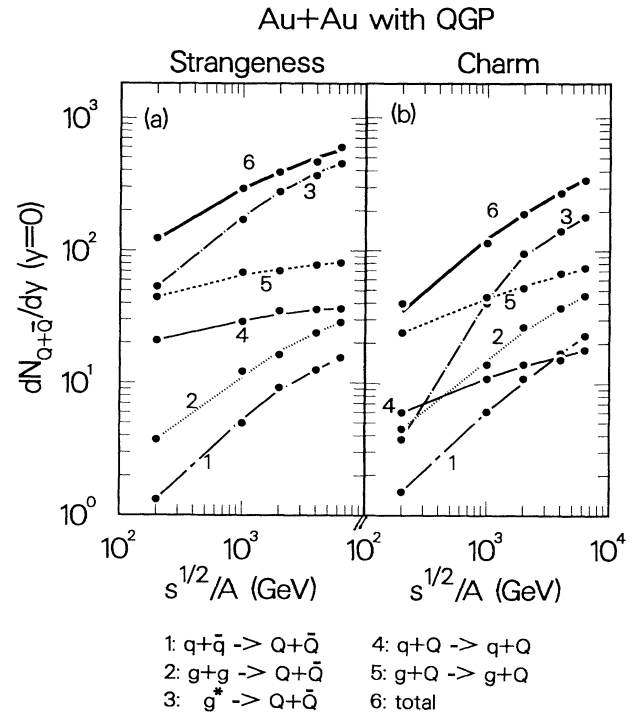


FIG. 3. Individual contributions from the processes (1)–(5) to the central rapidity density of (a) strange and (b) charm quarks plus antiquarks as a function of \sqrt{s}/A for the case of Au+Au collisions with plasma formation [cf. Fig. 2(a)].

drastic multiplicity increase at high energies.

The abundance of strange particles is a well-known dense matter signal, discussed in detail in [18,19]. In a hot, gluon dominated plasma there should be no significant difference between u , d , and s quark production, because the common thermal mass $m_u^{\text{th}} = m_d^{\text{th}} = m_s^{\text{th}} \propto gT$, acting as a production threshold is at high temperatures larger than the current quark masses, $m_q < m_q^{\text{th}}$. Indeed, as will be shown in Sec. III C below, the ratio of produced strange to light-quark-antiquark pairs increases from 0.7 (RHIC) to 1 (LHC). An enhanced charm production on the other hand has been advocated to serve as a sensitive thermometer for the initial temperature of QGP [7,8,24]. In fact, in the calculations presented here, the majority of charm quarks from $c\bar{c}$ production (which according to Fig. 3 provide the dominant contribution to the total charm yield) is due to the large number of energetic gluons with several GeV energy momentum. These gluons are mostly produced in primary parton collisions at very early times $\tau \lesssim 0.3$ fm and provide the main source of $c\bar{c}$ pairs. Therefore the charm quarks should have the momentum distribution of the gluons during the preequilibrium stage and upon thermalization, so that they reflect the initial temperature $T_0 \simeq T_g(\tau_0)$ around the plasma formation time τ_0 . The same argument holds also for $b\bar{b}$ creation, however this production rate is by more than an order of magnitude smaller and therefore more difficult to measure with sufficiently good statistics.

B. Momentum distributions

The rapidity and transverse momentum distributions of s and c quarks produced in central Au+Au collisions with plasma formation at RHIC and LHC energies are shown in Figs. 4 and 5, respectively. The thick curves represent the total yield resulting from the sum of the processes (1)–(5), the thin curves exhibit the contribution from the flavor creation processes (1)–(3) alone, and the difference of the curves is the contribution from the flavor excitation processes (4) and (5). The flavor creation via $s\bar{s}$ ($c\bar{c}$) production is concentrated in the central rapidity intervals $|y| \lesssim 2$ at $\sqrt{s} = 200$ A GeV, and $|y| \lesssim 3$ at $\sqrt{s} = 6300$ A GeV, wherein about 90% of the pairs are created. The quarks produced by flavor excitation extend to larger rapidities and widen the y distributions. The flavor creation processes also dominate the low p_\perp region with an exponential decrease, while the flavor excitation processes involve generally a larger transverse momentum and give rise to a power-law tail at large p_\perp . The different behavior of flavor creation and excitation processes can be understood as follows. The flavor creation of $Q\bar{Q}$ pairs results mainly from relatively hard collisions involving primary partons, either directly via gg fusion and $q\bar{q}$ annihilation, or indirectly via decay of massive virtual gluons produced in hard scatterings. In these processes a considerable fraction of the partons' energy is converted into the masses of the produced Q and \bar{Q} . Consequently the flavor creation processes happen preferably at smaller rapidity and lower p_\perp than the

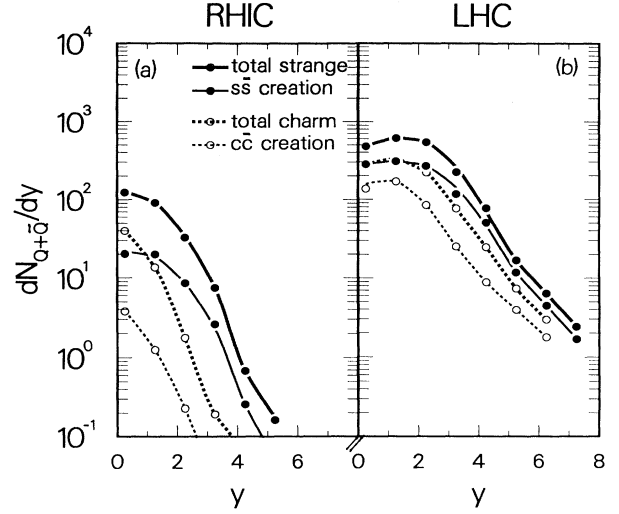


FIG. 4. Rapidity distributions of s and c quarks plus antiquarks produced in central Au+Au collisions with plasma formation at RHIC (LHC) energy, $\sqrt{s} = 200$ (6300) A GeV. The solid curves represent the total yield resulting from the sum of the processes (1)–(5), the thin curves exhibit the contribution from the flavor creation processes (1)–(3) alone.

flavor excitation processes.

Since, as argued before, the momentum spectrum of charm quarks should reflect the gluon momentum distribution up to τ_0 , the formation time for local equilibration of gluons, one may extract estimates for effective initial temperatures by a simple fit to the p_\perp spectra of $c\bar{c}$ pairs with a standard Fermi-Dirac distribution $\propto [\exp(-\sqrt{p_\perp^2 + m_Q^2}/T_0) + 1]^{-1}$. This yields initial temperatures $T_0^{\text{RHIC}} \simeq T_{c\bar{c}} = 600$ MeV at $\sqrt{s} = 200$ A GeV and $T_0^{\text{LHC}} \simeq T_{c\bar{c}} \simeq 900$ MeV at $\sqrt{s} = 6300$ A GeV.

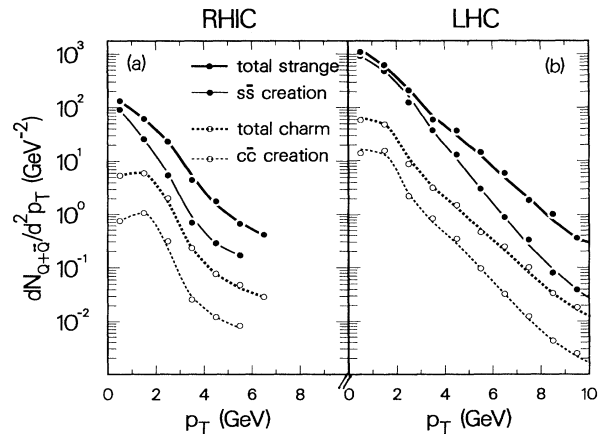


FIG. 5. Transverse momentum distributions of s and c quarks plus antiquarks produced in central Au+Au collisions with plasma formation at RHIC (LHC) energy, $\sqrt{s} = 200$ (6300) A GeV, in correspondence to Fig. 4.

C. Formation times and initial plasma temperatures

A perhaps more quantitative, and independent method to extract the initial plasma temperatures T_0 is to compare the parton cascade results in Au+Au collisions of Fig. 2(a) with the multiplicities of produced s and c quarks expected from an ideal QGP. The thermal production of Q and \bar{Q} from an ideal plasma in central AA collisions can be cast in the form [24]

$$R_Q^{\text{th}}(T) = \frac{T^6}{(2\pi)^4} \sum_k \sum_{a,b} \gamma_{ab} \int_{z_0}^{\infty} dz z^4 K_1(z) \hat{\sigma}_{ab \rightarrow Q}^{(k)} X(E) , \quad (14)$$

where $z = E/T$, $z_0 = 2m_Q/T$, and K_1 is the Bessel function of order one. In the sum over processes k , I will include [39] the $2 \rightarrow 2$ reactions (1), (2), (4), and (5) with the respective cross sections $\hat{\sigma}_{ab \rightarrow Q} X$ from Cambridge [27] as before. The degeneracy factors γ_{ab} involve summing over all initial spin, color, and flavor combinations. In order to relate the thermal yield (13) to the yield (11) from the parton cascade calculations of Fig. 2(a), I chose the formation time τ_0 equal to the relaxation time τ_{relax} associated with the entropy production in the central region [10] and extracted from the simulation:

$$\tau_0 \equiv \tau_{\text{relax}}(s) = \begin{cases} 0.40 \text{ fm}, & \sqrt{s} = 200 \text{ A GeV}, \\ 0.35 \text{ fm}, & \sqrt{s} = 1000 \text{ A GeV}, \\ 0.32 \text{ fm}, & \sqrt{s} = 2000 \text{ A GeV}, \\ 0.29 \text{ fm}, & \sqrt{s} = 4000 \text{ A GeV}, \\ 0.25 \text{ fm}, & \sqrt{s} = 6300 \text{ A GeV}. \end{cases} \quad (15)$$

Furthermore, using $T_c = 160$ MeV (at high initial temperatures T_0 the exact choice of T_c is not important) and $R_{\text{Au}} = 6.6$ fm, one obtains the thermal yield $dN_{Q+\bar{Q}}^{\text{th}}/dy$ as a function of initial temperature T_0 alone. Equating the rapidity density of the parton cascade calculations (11) with the thermal density (13),

$$\frac{dN_{Q+\bar{Q}}}{dy}(s) = \frac{dN_{Q+\bar{Q}}^{\text{th}}}{dy}(T_0) , \quad (16)$$

and solving for T_0 gives

$$T_0(s) = \begin{cases} 685 \text{ MeV}, & \sqrt{s} = 200 \text{ A GeV}, \\ 785 \text{ MeV}, & \sqrt{s} = 1000 \text{ A GeV}, \\ 850 \text{ MeV}, & \sqrt{s} = 2000 \text{ A GeV}, \\ 905 \text{ MeV}, & \sqrt{s} = 4000 \text{ A GeV}, \\ 970 \text{ MeV}, & \sqrt{s} = 6300 \text{ A GeV}. \end{cases} \quad (17)$$

It is worth noting that these rather high initial temperatures are in agreement with previous investigations [10,11], where the temperatures were inferred from the ratio of the partons' central energy density to entropy density. Also, Shuryak [7], as well as Biró *et al.* [9], find

$$\frac{dN_{Q+\bar{Q}}^{\text{th}}}{dy} = 3\pi R_A^2 \tau_0^2 T_0^6 \int_{T_c}^{T_0} \frac{dT}{T^7} [R_Q^{\text{th}}(T) + R_{\bar{Q}}^{\text{th}}(T)] , \quad (13)$$

where T_0 is the initial plasma temperature at formation time τ_0 and T_c is the critical temperature of the hadronic phase transition. The total production rate of quarks Q at temperature T , $R_Q^{\text{th}}(T)$, is, in lowest order perturbative QCD, given by

qualitatively similar estimates from different approaches.

The dependence of T_0 on $dN_{Q+\bar{Q}}/dy$ is plotted in Fig. 6(a) for $Q = s, c, b$, whereas in Fig. 6(b) the ratios

$$\rho_{Q+\bar{Q}}(s) = \frac{dN_{Q+\bar{Q}}/dy}{\frac{1}{2} (dN_{u+\bar{u}}/dy + dN_{d+\bar{d}}/dy)} \Big|_{y=0} \quad (18)$$

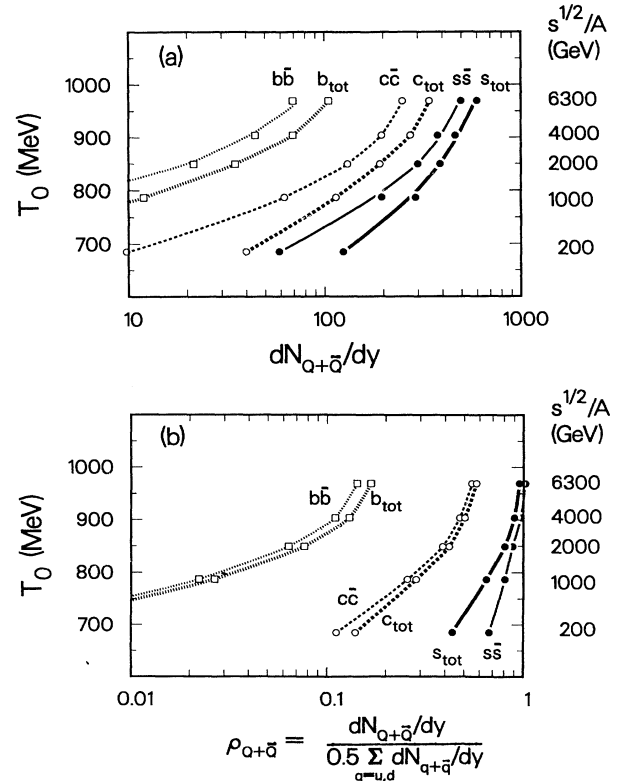


FIG. 6. Interrelation between initial temperatures T_0 at the time of local plasma formation in the central region, and (a) the rapidity densities $dN_{Q+\bar{Q}}/dy$, as well as (b) the ratios $\rho_{Q+\bar{Q}}$ defined in Eq. (18), around $y = 0$.

are shown. The figure suggests to infer the initial temperature T_0 by simply measuring the total strange or charm yield in the central rapidity region. Although it is to date not completely understood how these absolute multiplicities are reflected in the final hadron spectra, the ratios (18) in Fig. 6(b) of s , c , and b quarks to the light quarks should be equal in magnitude to the measurable ratios of strange, charm, and bottom mesons to pions, respectively, because of entropy conservation.

D. A dependence of heavy quark yields

The A dependence of quark production in high energy AA collisions is of interest, because with growing size of the collision system nuclear and medium effects [13,28], such as parton shadowing, the saturation of the gluon density, and the Landau-Pomeranchuk-Migdal effect, will play an increasingly prominent role. In Fig. 7 the calculated A dependence of strangeness, charm, and bottom production in central Au+Au collisions at RHIC [Fig. 7(a)] and LHC [Fig. 7(b)] energies. The solid curves depict the total yield from the flavor creation plus flavor excitation processes (1)–(5), and the dotted curves represent the contribution from the $Q\bar{Q}$ creation processes (1)–(3) alone. Generally, the multiplicities increase very strongly from pp to medium sized systems and show a saturation behavior for heavy nuclei. This saturation effect is naturally more prominent, the lighter the quarks are, and also increases with beam energy. For instance, in Au+Au collisions, the $s\bar{s}$ flavor creation has almost reached its limit at RHIC, whereas for $c\bar{c}$ creation the point of saturation lies at or beyond LHC energies. This

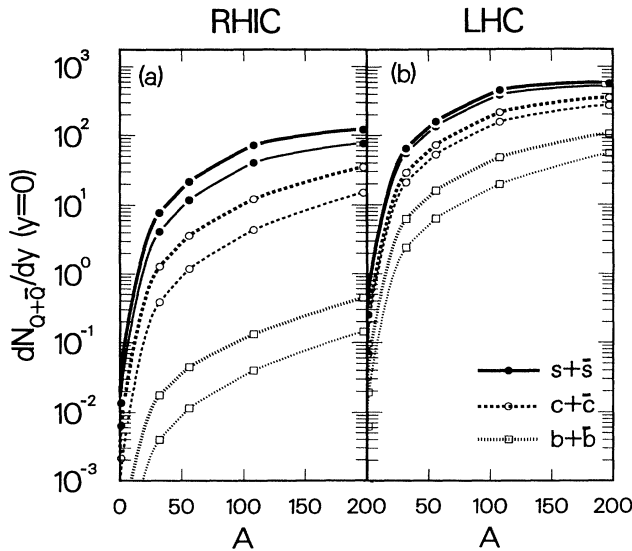


FIG. 7. A dependence of strangeness, charm, and bottom production in central Au+Au collisions at RHIC (a) and LHC (b) energies. The solid curves display the total yield from the flavor creation plus flavor excitation processes (1)–(5), and the dotted curves show the contribution from the $Q\bar{Q}$ creation processes (1)–(3) alone.

feature reflects the saturation of the gluon density in the central region already at very early times, since the initially produced hard gluons are mainly responsible for the $Q\bar{Q}$ creation. The point of maximum phase space density of the gluons depends on their energy momentum and therefore on the beam energy [15], so that the saturation of $Q\bar{Q}$ production acts as a meter for the maximum density of gluons with $E_g \simeq m_Q$.

The growth of the production cross section with A for particles of species P is conveniently parametrized by a power law in $\propto A^{\alpha_P}$ for pA collisions and $\propto A^{2\alpha_P}$ in AA collisions. The power α_P generally depends on the particle species P and on the beam energy \sqrt{s} [26], so that the multiplicity increase in central AA collisions may be related to pp collisions as

$$\frac{dN_P^{AA}}{dy} = A^{2\alpha_P(s)} \frac{dN_P^{pp}}{dy}. \quad (19)$$

From the calculated yields dN_P^{AA}/dy for $A = 1, 32, 56, 108, 197$ shown as data points in Fig. 7, I determined the values for $\alpha_P(s)$ for the total number of quarks plus antiquarks ($P = s + \bar{s}, c + \bar{c}, b + \bar{b}$), as well as for the contributions of the flavor creation processes alone ($P = s\bar{s}, c\bar{c}, b\bar{b}$), at $\sqrt{s} = 200 A$ GeV and $\sqrt{s} = 6300 A$ GeV. The results are listed in Table I. The values are remarkably close to the values for $P = \phi, J/\psi, \Upsilon$, determined from measured data of pA collisions $\alpha_\phi = 0.86 \pm 0.02$ [41], $\alpha_{J/\psi} = \alpha_{\psi'} = 0.92$, and $\alpha_\Upsilon = 0.97$ [42] (assumed to be independent of s).

The scaling behavior $\propto A^{1.6} - A^{1.9}$ implied by the α_P values of Table I and Eq. (19), yields a considerably stronger increase with A than the A dependence of Eq. (12), $\propto A^{1.1}$, which is based on the multichain model [36] and obtained from the number of individual nucleon-nucleon scatterings in AA collisions. The much stronger increase with A resulting from the parton cascade calculations, as compared to the case of purely hadronic interactions, is due to the larger number of quark-gluon degrees of freedom on the parton level, and the high density and temperature of the parton system. Therefore a measurement of the A dependence in the experiments at RHIC and LHC may provide another diagnostic tool for an indirect confirmation of a parton plasma formation.

TABLE I. The values of $\alpha_P(s)$ in Eq. (19) for the total number of quarks plus antiquarks ($P = s + \bar{s}, c + \bar{c}, b + \bar{b}$), as well as for the contributions of the flavor creation processes alone ($P = s\bar{s}, c\bar{c}, b\bar{b}$), at $\sqrt{s} = 200 A$ GeV and $\sqrt{s} = 6300 A$ GeV.

	$\alpha_P(s)$	$\alpha_{s+\bar{s}}$	$\alpha_{s\bar{s}}$	$\alpha_{c+\bar{c}}$	$\alpha_{c\bar{c}}$	$\alpha_{b+\bar{b}}$	$\alpha_{b\bar{b}}$
RHIC ($\sqrt{s} = 200 A$ GeV)	0.91	0.93	0.93	0.95	0.94	0.96	
LHC ($\sqrt{s} = 6300 A$ GeV)	0.80	0.80	0.82	0.83	0.84	0.85	

E. Resonance production of ϕ , J/ψ , ψ' , and Υ

From the previous considerations, one would expect that the copious production of strange, charm, and bottom quarks during the preequilibrium stage of heavy ion collisions should have a significant impact on the production rates of hadrons containing these quarks. In particular the substantial enhancement of the $s\bar{s}$, $c\bar{c}$, and $b\bar{b}$ flavor creation processes (1)–(3) should testify in the production rates of the vector meson resonances ϕ , J/ψ , ψ' , and Υ , and may provide an observable signal for a QGP formation. However, there are a number of uncertainties to be aware of. First, the mechanisms for the formation of these vector mesons from the quark-antiquark pairs are not yet completely understood, and second, the fate of these mesons while traversing the dense nuclear environment before escaping is rather unclear. Both these issues have been addressed for charmonium and bottomonium production within various models [19,22,42–45], with predictions ranging from significant suppression to substantial enhancement of resonance production in a QGP scenario. An experimental data analysis and investigative discussion of resonance production in relativistic AA collisions has recently been carried out by Vogt [40].

It is nevertheless of interest to estimate the resonance production rates of ϕ , J/ψ , ψ' , and Υ from the yields of s , c , or b quarks resulting from the parton cascade calculations, in connection with observable count rates in the heavy ion experiments at RHIC and LHC (discussed in Sec. III F below). Rather than pursuing a detailed model for resonance formation, I will follow an approach which is inspired by the simple picture advocated by Shor in Ref. [22]. The author assumes that in a QGP the coalescence of quarks with other partons in the plasma occurs at random, because the momenta and coordinates get quickly randomized [47], and furthermore that the binding between a quark and an antiquark is the same for all flavor combinations. Then the coalescence probabilities are simply determined by the relative particle abundances. This idea is compatible with the hadronization scheme developed for the parton cascade model in Ref. [13]. There the central idea is that at the end of the perturbative phase of parton cascade development, color singlet clusters of partons are formed which subsequently decay independently into hadrons. This concept is based on the “preconfinement” property [48], which is the tendency of the partons produced in the individual cascades to arrange in color singlet clusters with limited extension in both position and momentum space. It is natural to suppose that these clusters are the basic units out of which hadrons arise nonperturbatively. Within this cluster hadronization scheme the coalescence approach of Shor can be extended to a local description by discretizing phase space in cells and extracting the parton distributions in each cell individually, as described in Ref. [10]. Next, each gluon is represented by a light-quark-antiquark pair, so that one is left with a parton ensemble consisting only of quarks and antiquarks [13]. The local probability for the production of a ϕ , J/ψ , or Υ meson is now given by the multiplicity of $Q = s, c, b$ quarks in a certain phase-space cell times the probability that a

quark Q will find and coalesce with a \bar{Q} antiquark to form a $Q\bar{Q}$ bound state. This latter coalescence probability is taken to be the multiplicity of antiquarks \bar{Q} divided by the total multiplicity of partons in a given phase-space cell. Most of the time the Q will coalesce with a light antiquark to produce K , D , or B mesons. The relatively rare coalescence of $Q\bar{Q}$ states will yield primarily ϕ , J/ψ , or Υ , while the production of heavier resonances and higher spin states is considerably suppressed. The ψ' however will be accounted for by taking the relative probability of J/ψ to ψ' production to be 0.015 [49] at low energies and rising toward its asymptotic limit 0.25 [50]. Thus, the estimate for the total production of vector meson resonances $R = \phi, J/\psi, \psi', \Upsilon$ from coalescing $Q = s, c, b$ quarks and \bar{Q} antiquarks can be expressed as

$$N_R = \frac{1}{2} \sum_{\text{cells } k} [\langle n_Q(k) \rangle \mathcal{P}_{Q \rightarrow \bar{Q}}(k) + \langle n_{\bar{Q}}(k) \rangle \mathcal{P}_{\bar{Q} \rightarrow Q}(k)] , \quad (20)$$

where the sum runs over all phase-space cells k , $\langle n_a(k) \rangle$ is the event averaged number of partons of species a in cell k as extracted from the parton distributions F_a in the local rest frame of the cell [cf. Eq. (8)],

$$n_a(k) = \gamma_a \int_{\text{cell } k} \frac{d^3 r d^3 p}{(2\pi)^3} F_a(r, p) \quad (21)$$

and

$$\mathcal{P}_{Q \rightarrow \bar{Q}}(k) = \frac{\langle n_{\bar{Q}} \rangle}{\langle \sum_a n_a(k) \rangle} \quad (22)$$

is the probability that a quark Q would coalesce with an antiquark \bar{Q} in phase-space cell k .

Using this prescription and inserting the average multiplicities of partons in the central rapidity unit around $y = 0$, obtained from the simulations, one obtains the the rapidity densities $dN_R/dy|_{y=0}$ of resonances R . The resulting yield of ϕ , J/ψ , ψ' , and Υ is shown in Fig. 8(a) as a function of \sqrt{s}/A for central Au+Au collisions *with* plasma formation. In correspondence with Fig. 2(a), these particle yields reflect the copious $Q\bar{Q}$ production by the hot and dense parton matter in the central region of these reactions, with the effective initial temperatures T_0 , Eq. (17), associated with the beam energy \sqrt{s}/A .

Analogous to the procedure in Sec. III A, it is elucidating to compare these resonance yields with the multiplicities expected for purely hadronic interactions, that is, *without* plasma formation. To obtain an estimate for the latter, I employ the phenomenological parametrization of the hadronic production cross sections for resonances R in pp collisions [40,49]:

$$\left(\frac{d\sigma_R^{pp}}{dy} \right)_{y=0} = A_R \exp \left(-14.7 \frac{M_R}{\sqrt{s}} \right) , \quad (23)$$

where M_R is the resonance mass, and the normalizations are $A_\phi = 2400$ nb, $A_{J/\psi} = 500$ nb, $A_{\psi'} = 7.5$ nb, and $A_\Upsilon = 1.4$ nb. To extrapolate to AA collisions, I use the scaling behavior [24,25] [cf. Eq. (12)]

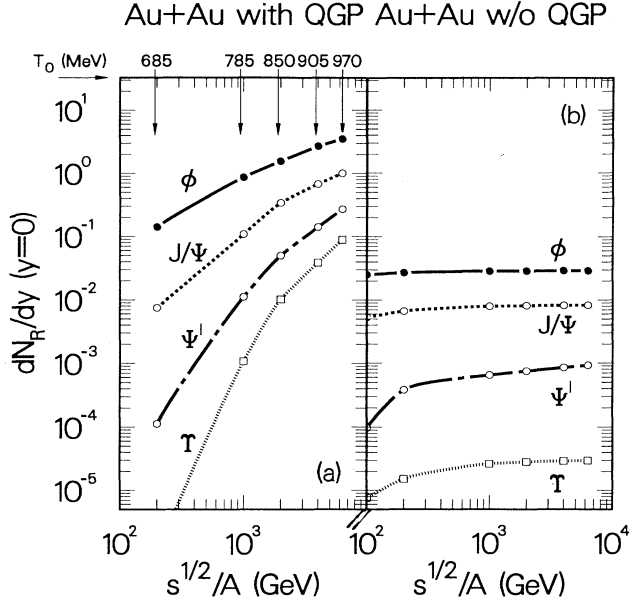


FIG. 8. Rapidity densities $dN_R/dy|_{y=0}$ of the vector meson resonances $R = \phi, J/\psi, \psi', \Upsilon$ as a function of \sqrt{s}/A for central Au+Au collisions: (a) *with* plasma formation, as obtained from the quark yields calculated with the parton cascade simulations of Au+Au collisions and on account of the coalescence approach, Eqs. (20)–(22); (b) *without* plasma formation, on the basis of individual nucleon-nucleon interactions, Eqs. (23) and (24), corresponding to resonance production exclusively due to primary parton-parton collisions without taking into account the contribution from interactions involving secondary partons and hard gluon bremsstrahlung.

$$\left(\frac{dN_R^{AA}}{dy}\right)_{y=0} = A^{\alpha_R+1/3} \frac{1}{\sigma_{\text{inel}}^{pp}} \left(\frac{d\sigma_R^{pp}}{dy}\right)_{y=0}, \quad (24)$$

with $\alpha_\phi = 0.86 \pm 0.02$ [41], $\alpha_{J/\psi} = \alpha_{\psi'} = 0.92$, and $\alpha_\Upsilon = 0.97$ [42], extracted from pA data, and $\sigma_{\text{inel}}^{pp}$, the inelastic cross section in pp collisions, is taken from [51]. This is the resonance yield that one would crudely expect in AA collisions without plasma formation, on the basis of individual nucleon-nucleon interactions [36,38]. As mentioned after Eq. (12), this corresponds in the parton language to resonance production exclusively due to primary parton-parton collisions and neglects the major contribution from interactions involving secondary partons and hard gluon bremsstrahlung. In this restricted case the number of parton interactions would also scale with the transverse size of the nuclear system, i.e., as $A^{2/3}$. The dependence of dN_R^{AA}/dy at $y = 0$ on the scaled beam energy \sqrt{s}/A is shown in Fig. 8(b).

In contrasting the two scenarios of Figs. 8(a) and 8(b), one observes that the resonance production is comparable at RHIC energy, but in case (a) increases so strongly that it exceeds the yield in scenario (b) by more than 2 orders of magnitude. Of course, these estimates are rather optimistic predictions, because it is assumed that all the $Q\bar{Q}$ bound states survive the plasma evolution

and the later stages of the nuclear collision. Nevertheless it shows that a considerable increase of resonance production can be expected in heavy ion collisions, if a high density, high temperature environment is created as predicted by the parton cascade simulations [10,11]. It is worth noting that the yields of $\phi, J/\psi, \psi'$, and Υ in Fig. 8(a) increase significantly faster with \sqrt{s}/A than the corresponding yields of s, c , and b quarks in Fig. 2(a). This effect arises, because the heavier the quarks Q the more likely they are to coalesce with much more abundant light antiquarks, instead of coalescing with the rare \bar{Q} antiquarks. However, the coalescence probabilities of Q and \bar{Q} grow considerably with \sqrt{s}/A , because, as is evident in Fig. 6(b), the ratios of heavy to light quark abundances increase.

F. Expectations for RHIC and LHC

One possibility to probe the vector meson resonance yield from the high density matter in the heavy ion experiments at RHIC and LHC, is to measure the count rates of lepton pairs produced by the decay of these resonances in the central rapidity region. To make a specific connection between the model predictions for the resonance yields dN_R/dy of Fig. 8(a) and the associated count rates of muon pairs in these experiments that would be implied by these predictions, two aspects have to be taken into consideration. First, whereas the model calculations were done by assuming ideally central AA collisions with impact parameter $b = 0$, the experimental definition of central collisions is always the average over a certain “central impact parameter” range. Second, one has to account for the luminosity of the collider beams. In order to incorporate these two points, it is convenient to express the total expected rate for resonance production $A + A \rightarrow R \rightarrow \mu^+\mu^-$ in AA collisions within a beam running time of 1.08×10^7 sec (one “experimental year” at RHIC or LHC) as [40]

$$N_R^{(\text{expt})} = 1.08 \times 10^7 L_{AA} B_R \sigma_R, \quad (25)$$

where L_{AA} is the beam luminosity, B_R is the branching ratio of the meson decays into $\mu^+\mu^-$ pairs, and σ_R is the total (integrated) resonance production cross-section for particles R . The measured cross section $B_R\sigma_R$ can be related to the number of produced particles per unit rapidity by

$$B_R \frac{d\sigma_R}{dy} = \sigma_{AA}(b_c) \left(C_R \frac{dN_R}{dy} \right). \quad (26)$$

Here

$$\sigma_{AA}(b_c) = \int_0^{b_c} d^2b \sigma_{pp}(b) T_{AA}(b) \quad (27)$$

is the total nuclear cross section integrated over the “central impact parameter” range b_c that depends on the experimentally achievable resolution. The normalization factor C_R is fixed by the ratio of the calculated total number of resonances N_R in pp collisions at $\sqrt{s} = 200$ GeV to

the corresponding measured number of $\mu^+\mu^-$ pairs that result from the leptonic decays of the resonances. The nuclear overlap integral in (27) is defined as

$$T_{AA}(b) = \int d^2r_{\perp} T_A(\mathbf{r}_{\perp}) T_A(\mathbf{b} - \mathbf{r}_{\perp}) \quad (28)$$

with the nuclear profile function

$$T_A(\mathbf{r}_{\perp}) = \int dz \rho_A(z, \mathbf{r}_{\perp}) \quad (29)$$

and the nuclear density distribution ρ_A is normalized as

$$\int d^3r \rho_A(\mathbf{r}) = 1 . \quad (30)$$

I will follow Ref. [40] to define the ‘‘central fraction’’ f_{AA} as

$$f_{AA}(b_c) = 2\pi \int_0^{b_c} db b T_{AA}(b) , \quad (31)$$

which is equivalent to the fraction of the total geometric cross section, πR_A^2 , involved in a central collision. Thus, for $b_c \ll 2R_A$, it follows, with Eq. (27), that

$$\sigma_{AA}(b_c) \approx \sigma_{AA}(0) \int_0^{b_c} d^2b T_{AA}(b) = \pi R_A^2 f_{AA}(b_c) , \quad (32)$$

and, using Eq. (26), one can rewrite the formula (25) as the expected binned production rate per unit rapidity for resonances R as

$$\begin{aligned} \frac{dN_R^{(\text{expt})}}{dy}(b_c) &= 1.08 \times 10^7 L_{AA} f_{AA}(b_c) (\pi R_A^2) \left(C_R \frac{dN_R}{dy} \right) . \end{aligned} \quad (33)$$

Inserting the estimated values dN_R/dy resulting from the full Au+Au simulations and on the basis of Eq. (20), I obtain the predictions listed in Table II for ϕ , J/ψ , ψ' , and Υ production that may be measured at RHIC and LHC. Here I used the quoted values for the beam luminosities at RHIC [52] and LHC [53] at maximum achievable $\sqrt{s}/A = 200$ GeV, respectively, $\sqrt{s}/A = 6300$ GeV. Listed are the results for both the central rapidity densities $dN_R^{(\text{expt})}/dy$ and the total integrated rates $N_R^{(\text{expt})}$, each for two different central impact parameters $b_c = 2$ fm and $b_c = 0.5$ fm with the corresponding central fractions f_{AA} taken from Ref. [40].

Such high resonance production rates as in Table II would be very promising. The ϕ meson rates however are also subject to a large background, because of accidental coincidences of $\pi^+\pi^-$ and K^+K^- decays, thermally produced lepton pairs and semileptonic decays of charmed particles in the mass region 1–3 GeV. The J/ψ and ψ' production rates should be high enough to be separately observable with sufficiently good statistics, since the background afflicting the ϕ is reduced in the J/ψ region. The Υ yield is probably not large enough at RHIC

TABLE II. Estimates for ϕ , J/ψ , ψ' , and Υ production that may be measured at RHIC and LHC in the invariant mass spectrum of muon pairs produced by the meson decays. The values for L_{AA} are the beam luminosities quoted for Au beams at RHIC [52] and Pb beams at LHC [53] at maximum achievable $\sqrt{s_{\text{max}}}/A$. Listed are the results for both the central rapidity densities $dN_R^{(\text{expt})}/dy$ and the total integrated rates $N_R^{(\text{expt})}$, each for two different central impact parameters $b_c = 2$ fm and $b_c = 0.5$ fm with the corresponding central fractions f_{AA} [40].

Quantity	Resonance production rates in Au+Au collisions per 3000 h			
	RHIC		LHC	
	200 GeV		6300 GeV	
$\sqrt{s_{\text{max}}}/A$				
L_{AA}	$2.0 \times 10^{26} \text{ cm}^{-2} \text{ s}^{-1}$		$6.0 \times 10^{26} \text{ cm}^{-2} \text{ s}^{-1}$	
b_c	2.0 fm	0.5 fm	2.0 fm	0.5 fm
f_{AA}	0.09	0.01	0.09	0.01
	$(dN_R^{(\text{expt})}/dy)_{y=0}$			
ϕ	1.28×10^6	1.42×10^5	9.81×10^7	1.09×10^7
J/ψ	7.66×10^4	8.51×10^3	3.21×10^7	3.57×10^6
ψ'	1.15×10^3	1.28×10^2	8.28×10^6	9.20×10^5
Υ	3.29×10^1	3.65×10^0	1.04×10^6	1.15×10^5
	Total $N_R^{(\text{expt})}$			
ϕ	4.38×10^6	4.87×10^5	3.38×10^8	3.75×10^7
J/ψ	2.13×10^5	2.37×10^4	8.92×10^7	9.91×10^6
ψ'	2.99×10^3	3.32×10^2	2.15×10^7	2.39×10^6
Υ	7.45×10^1	8.28×10^0	2.35×10^6	2.61×10^5

to provide a clean signal, but at LHC, where several thousand are produced, the Υ should show up clearly in the invariant mass spectrum of muon pairs.

G. Uncertainties and open questions

A general discussion concerning the assumptions and approximations of the parton cascade model can be found in Ref. [10]. Nevertheless some explanatory comments on the results for flavor production presented here are appropriate at this point. The rather large multiplicities of Q and \bar{Q} quarks produced in Au+Au collisions, evident in Fig. 2(a) and Fig. 3, may seem surprising at first sight. However, the separation of the various production processes in Fig. 3 exhibits some interesting features that elucidate the origin of this intense flavor production: (i) the Q (\bar{Q}) flavor production is overwhelmingly driven by the gluonic processes $g^* \rightarrow Q\bar{Q}$, $gg \rightarrow Q\bar{Q}$, and $gQ \rightarrow g\bar{Q}$; (ii) among the $2 \rightarrow 2$ processes, the *flavor excitation* process (5), $gQ \rightarrow g\bar{Q}$, outweighs the *flavor creation* process (2), $gg \rightarrow Q\bar{Q}$, over the entire displayed energy range, although the latter contribution rises steeply with \sqrt{s}/A and becomes comparable in magnitude at and beyond LHC energy; (iii) the $1 \rightarrow 2$ *flavor creation* process (3), $g^* \rightarrow Q\bar{Q}$, gives the dominant contribution for large energies ($\sqrt{s}/A \gtrsim 1$ TeV).

The first property (i) arises from the combination of two effects: first, the comparably large initial gluonic component in the nuclear structure functions [54,55], and second, the well-known property of perturbative QCD [56,57,7,11] that the amplitudes for the gluonic processes (2), (3), and (5), clearly outweigh those involving quarks only, (1) and (4), especially in the small angle region. The second point (ii) is also related to the initial partonic substructure of the incident nuclei, i.e., the fact that there is a significant strangeness and charm content in the sea quark contribution [54,55] to the nucleon structure functions $f(x, Q_0^2)$ at small energy fractions x and the ‘‘initial resolution scale’’ Q_0^2 [28]. For example, the structure function parametrization of Ref. [55] employed here gives relative proportions of $d : u : s : c$ quarks and antiquarks of 1.32:1.21:0.67:0.15 at RHIC ($\sqrt{s}/A = 200$ GeV, $Q_0 = 2.28$ GeV), and 2.28:2.11:1.17:0.26 at LHC ($\sqrt{s}/A = 6300$ GeV, $Q_0 = 5.23$ GeV) [28]. Therefore, in heavy ion collisions at RHIC energy and above, this incidently present component of spacelike virtual s and c sea quarks leads to a considerable materialization of strangeness and charm due to the frequent *flavor excitation* processes (4) and (5), which is obviously more favorable than the creation of new $s\bar{s}$ or $c\bar{c}$ pairs via $q\bar{q}$ annihilation (1) and gg fusion (2). This feature was already investigated by Combridge [27] in the context of strangeness production in hadronic collisions, who pointed out the uncertainties of flavor production connected with the nucleon structure functions of the initial state. Finally, the third point (iii) seems most stunning, in that the decays of timelike virtual gluons yield the increasingly dominant contribution to the flavor production in AA collisions at $\sqrt{s}/A \gtrsim 1$ TeV. From Fig. 3 it is obvious that these processes are responsible for the main part of $Q\bar{Q}$ production and the steep rise of $dN_{Q+\bar{Q}}/dy$

with collider energy. In the parton cascade model the cumulation of the processes $g^* \rightarrow Q\bar{Q}$ corresponds to the sum of all inelastic contributions in the leading logarithmic approximation [15], which are usually termed ‘‘higher twist’’ effects. The origin of these contributions lies in the early production of a large number of timelike gluons (mainly through inelastic primary parton collisions) with virtualities of a few GeV, which subsequently decay into two gluons or a quark-antiquark pair. Although the ratio of $g^* \rightarrow s\bar{s}$ ($c\bar{c}$) to $g^* \rightarrow gg$ is only about 3×10^{-2} (1.5×10^{-3}), almost independent of collider energy, the inelastic processes $g^* \rightarrow Q\bar{Q}$ occur frequently enough to be more favorable than the direct production via the elastic processes $gg \rightarrow Q\bar{Q}$. In this context I would like to refer also to the work of Biro, Levai, and Muller [58] who investigated strangeness production by gluonic processes in a QGP involving gluons that are effectively massive due to medium effects. The authors also find, however, within a more phenomenological approach, that the one-gluon decay process dominates for gluon masses above 300 MeV.

One might wonder about unitarity: the sum probabilities of all elastic and inelastic production channels should not exceed unity, or else one is in trouble. In the parton cascade model the conservation of unitarity is ensured by the recent implementation of the Levin-Ryskin unitarity condition [15], which may be represented in terms of the probability for producing a quark (antiquark) of type Q (\bar{Q}):

$$W_Q(r) = \frac{1}{\pi R_0^2} \left\{ n_\alpha(r) n_\beta(r) \hat{\sigma}_{\alpha\beta \rightarrow Q\bar{Q}} + \sum_{k=1}^{\infty} \prod_{i=1}^k n_{g_i^*}(r) \frac{\hat{\Gamma}_{g_i^* \rightarrow Q\bar{Q}}}{M_{g_i^*}} \right\} \equiv W_Q^{(\text{el})}(r) + W_Q^{(\text{inel})}(r), \quad (34)$$

such that

$$W_Q(r) \leq 1. \quad (35)$$

Here $n_\alpha(r) \equiv n_\alpha(\mathbf{r}, t)$ is the local, time-dependent density of partons of type α , $\hat{\sigma}_{\alpha\beta \rightarrow Q\bar{Q}} \propto \alpha_s^2/p_\perp^2$ is the elastic $2 \rightarrow 2$ scattering cross section, $\hat{\Gamma}_{g_i^* \rightarrow Q\bar{Q}} \propto \alpha_s/M_{g_i^*}$ the decay width of timelike excited gluons with virtuality $M_{g_i^*}$, and R_0 is taken to be 1 fm, the typical hadronic scale. For the collider energies range considered here, even for Au+Au collisions this probability is at most $W_s^{\text{max}} \simeq 0.04$ (0.13) and $W_c^{\text{max}} \simeq 0.01$ (0.03) at $\sqrt{s}/A = 200$ (6300) GeV. On the other hand, the corresponding probability for producing gluons,

$$W_g(r) = \frac{1}{\pi R_0^2} \left\{ n_\alpha(r) n_\beta(r) \hat{\sigma}_{\alpha\beta \rightarrow gX} + \sum_{k=1}^{\infty} \prod_{i=1}^k n_{g_i^*}(r) \frac{\hat{\Gamma}_{\alpha_i^* \rightarrow gX}}{M_{\alpha_i^*}} \right\}, \quad (36)$$

where $\alpha^* = g^*(q^*)$, at times approaches unity in the most densely populated phase-space of the central region,

which however is balanced by the increasing probability for the fusion processes $gg \rightarrow g^*$ [11].

Summarizing these considerations precautiously, I would like to state that the band of uncertainty in strangeness and charm production is bounded by curves 2 and 6 in Fig. 3, that is of roughly one order of magnitude. Curve 2 represents the lower limit for s and c production via the *flavor creation* process $gg \rightarrow Q\bar{Q}$ alone, neglecting the sizable but uncertain contributions of the *flavor excitation* processes associated with sea quark excitation, as well as the dominant inelastic *flavor creation* processes $g^* \rightarrow Q\bar{Q}$. Certainly the total s and c yield cannot be less than curve 2, which extrapolates without difficulty to the high energies considered. Curve 6, on the other hand, as the sum of all contributing processes, must be understood as a very optimistic upper bound that depends crucially on the magnitude of the dominant contributions 3 and 5. If indeed the true s and c yield in heavy ion collisions at RHIC and LHC comes close to the predicted curves 6, then the resulting K and especially D mesons should be experimentally detectable with outstanding multiplicities. If however the total s and c yield turns out to be only slightly larger than curve 2, then it is rather questionable if the strange and charmed mesons would be produced in appreciable numbers.

It should be noted that the total multiplicity of parton interactions is in general sensitively dependent on the two infrared regularization parameters [28] of the parton cascade model, namely, the minimum required momentum transfer in parton-parton collisions, $p_{\perp\text{cut}}$, and the minimum required virtuality for a parton to decay, μ_0 . However, for $Q\bar{Q}$ (particularly for $c\bar{c}$ and $b\bar{b}$) production the threshold $2m_Q$ provides a natural cutoff that is above or of the order of $p_{\perp\text{cut}} = 1.55$ (3.95) GeV for RHIC (LHC) energy and $\mu_0 = 1$ GeV (independent of beam energy). Therefore the flavor production of the heavier quarks is far less sensitive to the choice of $p_{\perp\text{cut}}$ and μ_0 than the production of light quarks or low energy gluons.

In addition to the question of how the screening in the dense matter of heavy ion collisions might act as a natural infrared regularization and may modify the role of $p_{\perp\text{cut}}$ and μ_0 , there are a number of uncertainties involved in $Q\bar{Q}$ production, as has recently been investigated in detail by Mangano *et al.* [59]. Still, the results of the parton cascade calculations for pp collisions, indicated in Fig. 2(b) by the thin curves, agree well with the improved parton model predictions of [59] for charm and bottom production in pp collisions that fit the recent experimental data compilations on inclusive heavy flavor production [60] in hadron collisions. For example, the parton cascade model prediction for the total $c\bar{c}$ cross section at $\sqrt{s}/A = 200$ (6300) GeV is $\sigma_{c\bar{c}} = 0.63$ (5.9) mb with $m_c = 1.35$ GeV and the structure functions of [55]. This may be compared with the corresponding prediction of Mangano *et al.* [59] $\sigma_{c\bar{c}} \simeq 0.6$ (4.0) mb. Hence, the charm yield calculated with the parton cascade model for pp collisions is relatively accurate within the uncertainties associated with the exact value of m_c , the choice of the structure function parametrization, etc., so that any additional uncertainty in AA collisions is connected with the extrapolation from pp to AA , i.e., the lack of

detailed knowledge about nuclear and dense medium effects that are essential in AA reactions but are irrelevant in pp collisions.

From this discussion it should be clear that the predictions of the model calculations for AA collisions are to be understood more as qualitative results, and one must keep in mind that there are a number of fundamental questions that remain to be understood better in order to make accurate predictions. I believe, the two most important issues are (i) the *initial state*, the uncertainty in the magnitude of the gluonic and sea quark component in the nuclear structure functions at small x ($\lesssim 10^{-3}$) and (ii) *nuclear and medium effects*, the interpretation of the infrared cutoffs $p_{\perp\text{cut}}$ and μ_0 , which in pp collisions are constrained by experimental data, but in AA reactions must be related to the infrared behavior of partons in dense QCD matter (screening).

IV. SUMMARY AND CONCLUDING REMARKS

Within the framework of the parton cascade model, I have investigated the properties of strange, charm, and bottom quark production in central AA collisions at collider energies and discussed, on the basis of a coalescence approach, the possible observable consequences for the yields of the vector meson resonances ϕ , J/ψ , ψ' , and Υ containing these quarks. The dependence of the quark production on the beam energy over the range $\sqrt{s}/A = 200$ –6300 GeV, and on the size of the collision system ranging from pp to Au+Au, was studied. For the case of Au+Au collisions two scenarios were compared with and without plasma formation. The results of the realistic simulations with plasma formation predict a very optimistic scenario in heavy ion reactions at the RHIC and LHC experiments with very large abundances in the central region of strange, charm, and even bottom particles relative to pp collisions at the same energies. If indeed such a strong enhancement of heavy flavor production could be observed in these experiments, then, according to the present analysis, this would be a clear indication for the formation of a hot and dense parton plasma in the central collision region with initial temperatures considerably larger than commonly assumed in earlier studies. The results may be summarized as follows.

(i) Vehement entropy production by initially produced energetic gluons leads to very large abundances of s , c , and b quarks. In Au+Au collisions this particle production from the preequilibrium stage is generally more than an order of magnitude bigger than would be expected on the basis of purely hadronic interactions. The dominant contribution comes from flavor creation processes in the central rapidity unit, especially from decays of virtually excited gluons. The yields show a logarithmic increase with \sqrt{s} and the A dependence scales as $A^{2\alpha_P(s)}$ from pp to AA , with an energy dependent α_P ranging from $\simeq 0.8$ to $\simeq 1$ for $P = s, c, b$.

(ii) The ratio of the production rates of strange to light quark-antiquark pairs is already $\simeq 0.7$ at RHIC energy and approaches 1 at LHC. The analogous ratios of the

charm and bottom pair production in this energy range grow from $\simeq 0.1$ to $\simeq 0.5$, and from $\simeq 10^{-3}$ to $\simeq 0.1$, respectively. The copious production of these quarks in the central rapidity region adds on top of a significant suppression of partons in the initial nuclear wave functions due to nuclear shadowing, and due to medium effects that the partons encounter during their evolution in the dense plasma environment.

(iii) The sizable production of charm quarks, as well as with \sqrt{s} increasingly significant bottom yield, from gluons during the preequilibrium stage may serve as a thermometer of the initial temperature of a gluon dominated plasma upon formation time, simply by measuring the ratios of the numbers of resulting charmed mesons D , J/ψ , ψ' (at LHC also the bottom mesons B, Υ) to light hadrons. The initial plasma temperatures estimated from the calculated quark yields in Au+Au collisions range from $T_0(s) = 685\text{--}970$ MeV for $\sqrt{s}/A = 200\text{--}6300$ GeV.

(iv) The vector meson resonance production of ϕ , J/ψ , ψ' , and Υ that results from coalescing quarks and antiquarks produced in close proximity of momentum and coordinate space, show a steep increase with \sqrt{s} and associated initial plasma temperatures. In Au+Au collisions at RHIC, the resonance yields from preequilibrium and early plasma are still comparable in magnitude with those expected from a simple scaling extrapolation of hadron collisions, but at LHC an enhancement of more than 2 orders of magnitude might show up. The estimated count rates for ϕ and J/ψ would be large enough already at RHIC energy to be measurable with sufficient statistics in the spectra of dileptons produced by the meson decays. At LHC even the Υ should be produced in several thousands over the time of an “experimental year”.

I emphasize once more that the results presented in this paper are to be understood as *qualitative* features associated with ultradense, high temperature parton matter produced in the central collision region of heavy ion collisions at collider energies. As stressed repeatedly, the calculations and results presented in this paper must be viewed as an optimistic upper limit of the possible flavor yield that is subject to considerable uncertainties. Especially, more experimental and theoretical information is necessary regarding the heavy flavor sea excitation and glue decay production at RHIC and LHC energies in order to draw robust conclusions for the experimentally observable heavy flavor yield. However, if the underlying description of the partons’ kinetics in these reactions is tendentially correct, then the results should nevertheless have predictive power. Nevertheless, accurate *quantitative* predictions for experimental signatures require further understanding of a number of issues on both the perturbative evolution of partons and the nonperturba-

tive mechanisms of hadron formation. Most urgent on the perturbative sector is the medium modification of the parton interaction amplitudes. This open problem is intimately connected to the choice of the model parameters $p_{\perp \text{cut}}$ and μ_{cut} , used to regularize the divergent perturbative QCD parton-parton cross sections and the parton emission probabilities, respectively. The energy dependent values of these parameters, fixed from experimental data on e^+e^- annihilation and hadron-hadron collisions, are so far taken to be universal, that is, independent of the reaction. The rather low values of $p_{\perp \text{cut}}$ and μ_{cut} in the model reproduce well a wide range of pp ($p\bar{p}$) collider data, but lead to a huge multiplicity growth of partons when proceeding to heavy ion reactions. Since the parton-parton cross sections and emission probabilities depend sensitively on $p_{\perp \text{cut}}$ and μ_{cut} , an increase of these cutoff parameters due to dense medium effects would lead to significantly more moderate particle production. Therefore it is important to investigate the color screening length as well as effective medium induced masses of collective gluon and quark modes as a function of space and time. These quantities could then be used as input parameters for the determinations of medium dependent scattering cross sections and parton branching probabilities. This would provide a *natural* cutoff of long-range interactions in a deconfined QCD plasma, so that no artificial parameters are required to obtain finite interaction amplitudes in a dense medium. One possible way of approach could be to relate the average impact parameter in parton-parton collisions via Fourier transformation to the minimum encountered transverse momentum involved in the scatterings. Since with increasing particle density the mean impact parameter would decrease, the corresponding $p_{\perp \text{cut}}$ values would increase and provide a self-consistent regularization of infrared divergences. Accordingly, the maximum occurring value of the QCD coupling $\alpha_s^{\text{max}} = \alpha_s(p_{\perp \text{cut}}^2)$ would be a space-time dependent function of the particle density, with its decrease dictating the effect of color screening. Thus, a natural cutoff would be determined by the parton dynamics itself [61].

ACKNOWLEDGMENTS

The parton cascade simulations were performed on the Cray computers of the Minnesota Supercomputer Institute and on a Silicon Graphics computer at Duke University. This work was supported by the U.S. Department of Energy under Grant No. DOE/DE-FG02-87ER-40328.

[1] For a recent overview, see *Quark Matter '91*, Proceedings of the Ninth International Conference on Ultra-relativistic Nucleus-Nucleus Collisions, Gatlinburg, Tennessee, 1991, edited by T. C. Awes *et al.* [Nucl. Phys.

A544, 1c (1992)].

[2] B. Müller, in *Particle Production in Highly Excited Matter*, edited by H. Gutbrod and J. Rafelski (Plenum, New York, 1993).

- [3] *Quark Gluon Plasma*, edited by R. C. Hwa (World Scientific, Singapore, 1990).
- [4] E. V. Shuryak, Phys. Lett. **78B**, 150 (1978); Yad. Fiz. **28**, 796 (1978) [Sov. J. Nucl. Phys. **28**, 408 (1978)].
- [5] C. P. Singh, Int. J. Mod. Phys. **A 29**, 7185 (1992).
- [6] *Quark Gluon Plasma Signatures*, Proceedings of the International Workshop on Quark Gluon Plasma Signatures, Strasbourg, France, 1991, edited by V. Bernard *et al.* (Editions Frontières, Gif-sur-Yvette, France, 1991).
- [7] E. V. Shuryak, Phys. Rev. Lett. **68**, 3270 (1992).
- [8] B. Müller and X.-N. Wang, Phys. Rev. Lett. **68**, 2437 (1992).
- [9] T. S. Biró, E. van Dorn, M. H. Thoma, B. Müller, and X.-N. Wang, Phys. Rev. D **48**, 1275 (1993).
- [10] K. Geiger, Phys. Rev. D **46**, 4965 (1992); **46**, 4986 (1992).
- [11] K. Geiger and J. I. Kapusta, Phys. Rev. D **47**, 4905 (1993).
- [12] K. Geiger and B. Müller, Nucl. Phys. **B369**, 600 (1992).
- [13] K. Geiger, Phys. Rev. D **47**, 133 (1993).
- [14] I. Kaurakow, H.-J. Möhring, and J. Ranft, in *Quark Matter '91* [1], p. 471c.
- [15] E. M. Levin and M. G. Ryskin, Phys. Rep. **189**, 267 (1990); L. V. Gribov, E. M. Levin, and M. G. Ryskin, *ibid.* **100**, 1 (1983).
- [16] A. Bialas and J.-P. Blaizot, Phys. Rev. D **32**, 2954 (1985); J. Kapusta, L. McLerran, and D. K. Srivastava, Phys. Lett. B **283**, 145 (1992); B. Kämpfer and O. P. Pavlenko, *ibid.* **289**, 127 (1992); I. Kaurakow and J. Ranft, University of Leipzig Report No. UL-HEP-92-08 (unpublished); E. Shuryak and L. Xiong, Phys. Rev. Lett. **70**, 2241 (1993).
- [17] K. Geiger and J. I. Kapusta, Phys. Rev. Lett. **70**, 1290 (1993).
- [18] J. Rafelski, in *Quark Matter '91* [1], p. 279c; P. Koch, B. Müller, and J. Rafelski, Phys. Rep. **142**, 167 (1986).
- [19] J. Kapusta and A. Mekjian, Phys. Rev. D **33**, 1304 (1986); T. Matsui, B. Svetitsky, and L. D. McLerran, *ibid.* **34**, 783 (1986); **34**, 2047 (1986).
- [20] T. Matsui and H. Satz, Phys. Lett. B **178**, 416 (1986).
- [21] J.-P. Blaizot, in *Quark Gluon Plasma* [3], pp. 631, and references therein.
- [22] A. Shor, Phys. Lett. B **246**, 207 (1990).
- [23] J. Milana, Phys. Rev. Lett. **62**, 2921 (1989).
- [24] A. Shor, Phys. Lett. B **215**, 375 (1988); **233**, 231 (1989).
- [25] H. Satz, in *Quark Matter '91* [1], p. 371c.
- [26] S. J. Brodsky and P. Hoyer, Phys. Rev. Lett. **63**, 1566 (1989).
- [27] B. Combridge, Nucl. Phys. **B151**, 429 (1979).
- [28] K. Geiger, "Nuclear and Medium Effects for Hadron Production in Ultrarelativistic Heavy Ion Collisions," UMSI Report No. 92/174, University of Minnesota, 1992 (unpublished).
- [29] L. L. Frankfurt and M. I. Strikman, Phys. Rep. **160**, 235 (1988); F. E. Close, J. Qiu, and R. G. Roberts, Phys. Rev. D **40**, 2820 (1989); A. H. Mueller, Nucl. Phys. **B335**, 115 (1990); X. N. Wang and M. Gyulassy, Phys. Rev. Lett. **68**, 1480 (1992); K. Eskola, Nucl. Phys. **B400**, 240 (1993).
- [30] K. Kajantie, P. V. Landshoff, and J. Lindfors, Phys. Rev. Lett. **59**, 2527 (1987); K. J. Eskola, K. Kajantie, and J. Lindfors, Nucl. Phys. **B323**, 37 (1989).
- [31] X. N. Wang, Phys. Rev. D **43**, 104 (1991); X. N. Wang and M. Gyulassy, *ibid.* **44**, 3501 (1991).
- [32] L. D. Landau and I. Ya. Pomeranchuk, Dokl. Akad. Nauk SSSR **92**, 535 (1953); **92**, 735 (1953); N. N. Nikolalev, Usp. Fiz. Nauk **134**, 369 (1981) [Sov. Phys. Usp. **24**, 531 (1981)].
- [33] European Muon Collaboration, J. Ashman *et al.*, Phys. Lett. B **202**, 603 (1988); M. Arneodo *et al.*, *ibid.* **211**, 493 (1988).
- [34] R. K. Ellis and J. C. Sexton, Nucl. Phys. **B269**, 445 (1986).
- [35] N. Abou-El-Naga, K. Geiger, and B. Müller, J. Phys. G **18**, 797 (1992).
- [36] K. Kinoshita, A. Minaka, and H. Sumiyoshi, Z. Phys. C **8**, 205 (1981).
- [37] H. Cobiaert *et al.*, Phys. Lett. B **206**, 546 (1987); M. E. Duffy *et al.*, Phys. Rev. Lett. **55**, 1816 (1985).
- [38] This scaling behavior assumes that for central AA collisions $dN_{Q+\bar{Q}}^{AA}/dy = \bar{n} dN_{Q+\bar{Q}}^{pp}/dy$ [36], where $\bar{n} = A\bar{v}$ with \bar{v} the mean number of struck nucleons in pA collisions. In pA collisions the charm production cross section has been found to scale as $\sigma^{pA} = A^\alpha \sigma^{pp}$ with $\alpha = 0.76$ [37], so that $\bar{v} = (1/A^{2/3})(\sigma^{pA}/\sigma^{pp}) = A^{\alpha-2/3}$ and $\bar{n} = A^{\alpha+1/3}$.
- [39] Note that the bremsstrahlung process (3), $g \rightarrow Q\bar{Q}$, is not accounted for in Eq. (14). However, in a perfect thermal system the relative contribution of the process $gg \rightarrow Q\bar{Q}$ to the total $Q + \bar{Q}$ yield turns out to be about as large as the sum of contributions from $g \rightarrow Q\bar{Q}$ plus $gg \rightarrow Q\bar{Q}$ resulting from the parton cascade calculations. Therefore it should be justified to qualitatively compare the rates (11) and (13) of the two scenarios.
- [40] R. Vogt, At. Data Nucl. Data Tables **50**, 343 (1992).
- [41] R. Bailey *et al.*, Z. Phys. C **22**, 125 (1984).
- [42] D. M. Alde *et al.*, Phys. Rev. Lett. **66**, 133 (1991).
- [43] J. Cleymans and C. Vanderzande, Phys. Lett. **147B**, 186 (1984); H. J. Reusch, Z. Phys. C **26**, 105 (1984).
- [44] S. Gavin, M. Gyulassy, and A. Jackson, Phys. Lett. B **208**, 257 (1988); R. Vogt, M. Prakash, P. Koch, and T. H. Hansson, *ibid.* **208**, 263 (1988); J.-P. Blaizot and J.-Y. Ollitrault, Phys. Rev. D **39**, 232 (1989).
- [45] S. J. Brodsky and A. H. Mueller, Phys. Lett. B **206**, 685 (1988).
- [46] S. Gupta and H. Satz, Phys. Lett. B **283**, 439 (1992); Z. Phys. C **55**, 391 (1992).
- [47] B. Svetitsky, Phys. Rev. D **37**, 2428 (1988).
- [48] A. Bassetto, M. Ciafaloni, and G. Marchesini, Phys. Rep. **100**, 203 (1983).
- [49] N. S. Craigie, Phys. Rep. **47**, 1 (1978).
- [50] L. Lyons, Prog. Part. Nucl. Phys. **7**, 169 (1981).
- [51] K. Goulianos, in *Physics Simulations at High Energies*, edited by V. Barger *et al.* (World Scientific, Singapore, 1987).
- [52] *1989 RHIC Conceptual Design Report* (BNL Report No. 52195, Upton, New York, 1989).
- [53] J. Schukraft, talk given at the Workshop on a Dedicated Heavy Ion Detector for LHC, Geneva, Switzerland, 1993 (unpublished).
- [54] E. Eichten, I. Hincliffe, K. Lane, and C. Quigg, Rev. Mod. Phys. **56**, 579 (1984).
- [55] M. Glück, E. Reya, and A. Vogt, Z. Phys. C **48**, 471 (1990).
- [56] L. van Hove and S. Pokorski, Nucl. Phys. **B86**, 243 (1975).
- [57] E. Shuryak, Yad. Fiz. **28**, 796 (1978) [Sov. J. Nucl. Phys. **28**, 408 (1978)].
- [58] T. S. Biró, P. Lévai, and B. Müller, Phys. Rev. D **42**,

- 3078 (1990).
- [59] M. L. Mangano, P. Nason, and G. Ridolfi, "Fixed Target Hadroproduction of Heavy Quarks," Report No. IFUP-TH-37/92, INFN (unpublished).
- [60] J. Appel *et al.*, *Annu. Rev. Nucl. Part. Sci.* **42**, 367 (1993); L. Rossi, in *Proceedings of the 4th International Symposium on Heavy Flavor Physics*, Orsay, France, 1991, edited by M. Davier and G. Wormser (Editions Frontieres, Gif-sur-Yvette, 1992); E771 Collaboration, G. Introzzi, in *Heavy Flavor Physics*, Proceedings of the 3rd Topical Seminar, San Miniato, Italy, 1991 [*Nucl. Phys. B* (Proc. Suppl. (in press))].
- [61] This idea arose in discussions with J. Kapusta and B. Müller.